THE JOURNAL OF PHYSICAL CHEMISTRY A

Article

pubs.acs.org/JPCA

Classical Trajectory Study of Energy Transfer in Collisions of Highly Excited Allyl Radical with Argon

Riccardo Conte,*[,†] Paul L. Houston,*[,‡] and Joel M. Bowman*[,†]

[†]Department of Chemistry and Cherry L. Emerson Center for Scientific Computation, Emory University, Atlanta, Georgia 30322, United States

[‡]School of Chemistry and Biochemistry, Georgia Institute of Technology, Atlanta, Georgia 30332, United States

ABSTRACT: Predicting the results of collisions of polyatomic molecules with a bath of atoms is a research area that has attracted substantial interest in both experimental and theoretical chemistry. Energy transfer, which is the consequence of such collisions, plays an important role in gas-phase kinetics and relaxation of excited molecules. We present a study of energy transfer in single collisions of highly vibrationally excited allyl radical in argon. We evolve a total of 52 000 classical trajectories on a potential energy surface, which is the sum of an ab initio intramolecular potential for the allyl and a pairwise interaction potential describing the argon's effect on the allyl. The former is described by means of a permutationally invariant full-dimensional potential, whereas the interaction potential between allyl and argon is obtained by means of a sum of pairwise potentials dependent on nonlinear parameters that have been fit to a set of MP2/avtz counterpoise corrected ab initio energies. Results are reported for energy transfers and related probability densities at different collisional energies. The sensitivity of results to the interaction potential is considered and the potential is shown to be suitable for future applications involving different isomers of the allyl. The impact of highly efficient collisions in the energy transfer process is examined.

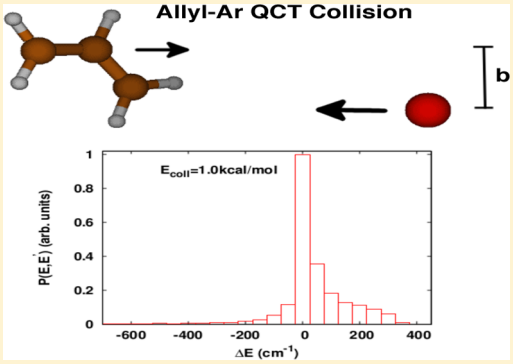

INTRODUCTION

Experimental as well as computational and theoretical work on collisions between chemical species is a topic of major interest in physical chemistry. Collisions may either relax an internally excited molecule, thereby quenching isomerization and unimolecular dissociation, or transfer energy to the target by means of multiple thermal events or single impulsive ones. Many different experimental studies have been performed in the past (see, for instance, refs 1−12) to investigate the energy-transfer process in collisions. A list of the principal experimental techniques employed includes kinetically controlled selective ionization (KCSI),[13] high-resolution transient IR absorption spectroscopy,[14,15] mass spectroscopy,[16] and time-sliced ion techniques.[17] Related topics of interest comprise the formation of collision complexes that are long-lived on the collision time scale and the impact of highly efficient collisions (HEC), often and even recently[11,17,18] referred to in the literature as "supercollisions", which are rare events in the tail of the distribution, thus characterized by a large amount of energy transfer (see, for instance, refs 14, 15, 19, and 20).

Energy transfer is a key component in master equations, from which temperature and pressure dependent rate coefficients may be derived for various different physical and chemical processes. Inaccuracy in determining the energy transfer is a primary source of error in master equation calculations, and many different aspects may influence the outcome. In fact, energy transfer has been found to be dependent on the interaction potential and the type of bath, in addition to depending on more straightforward quantities like internal and collision energy. In studies about its dependence on the bath gas, energy transfer has been shown to decrease as the mass of the bath increases, as predicted by the Landau−Teller theory, but on the other hand, the trend is inverted if the internal structure of the collider grows.[21−23] These competing effects can be explained by invoking two different kinds of energy transfer events. In the former case, there is impulsive V → T transfer with lighter molecules advantaged due to their higher velocity. When this kind of process dominates, the lighter molecule is a better quencher of the excited target. In the latter case, the type of process involved is a V → V transfer, so baths with complex inner structure are more likely to participate. The target molecule is expected to play an influential role in this type of collision.[24,25] Rotational energy transfer is also important as it may concern both the target and a polyatomic collider. T → R energy transfer from the collider to the target as well as the opposite process are observed when the molecule is given an initial rotational energy distribution. When dealing with polyatomic colliders, V → R energy transfer is also detected. In all cases, the initial total angular momentum must be conserved. Intense rotational energy transfer should be favored by higher impact parameter values but, on the other

Received: October 17, 2013
Revised: December 3, 2013
Published: December 3, 2013

   dx.doi.org/10.1021/jp410315r | J. Phys. Chem. A 2013, 117, 14028−14041

hand, the interaction mediating the energy transfer becomes weaker.

From a theoretical point of view, the study of the collisional process relies on the accurate description of the full-dimensional potential energy surface (PES) on which the collision takes place. However, the determination of a full-dimensional PES is computationally expensive, apart from the case of colliding systems composed of a very small number of atoms (usually not more than four or five), for which even quantum scattering studies are possible and in part have already been undertaken.[26−28] A possible way to overcome this issue has been recently proposed in a study of CH_4 colliding with different bath molecules.[29−31] These studies have been performed treating the electronic problem "on-the-fly", i.e., obtaining the electronic energy and gradient for the full-dimensional system from ab initio calculations at every step along the evolution of the direct dynamics. However, this approach cannot be easily used in connection with expensive high-level ab initio electronic calculations or to study low-probability events with good statistics. For instance, as we will demonstrate in the paper, the use of MP2/aug-cc-pvtz for the allyl−argon system is already out of reach for direct dynamics.

Collisions involving more complex molecules realistically need a classical treatment for the dynamics and the introduction of a reasonable representation of the PES. The first aspect implies neglecting tunneling effects, which are expected to be of minor importance due to the high density of vibrational states in the excited target, and zero-point energy leaking, which can be avoided when the initial conditions are prepared but may affect the relaxation process. As for the treatment of the full potential, it is generally written as a sum of an intramolecular one for the target molecule and an interaction one between the atom and the target, with the latter approximated by a sum of pairwise functions dependent on the distances between the collider and the atoms of the target molecule.[32−34] The effect of neglect of many body terms has been tested by means of direct dynamics on CH_4+M systems,[30] showing that the pairwise functional form is more reliable when the interaction potential is nearly isotropic.

The intramolecular potential has often been modeled using collections of simple analytical potentials, like harmonic or Morse-type oscillators to describe internal stretching, bendings, waggings and torsions.[35−38] These models have suggested that the intramolecular potential may not be critical to the average energy transfer,[32,39,40] but may be a factor on rare events like highly efficient collisions. The intermolecular potential is likewise important. In fact, the accuracy of the energy transfer is mainly associated with the capacity to reproduce correctly the repulsive wall.[41,42] However, a realistic description of the attractive part of the potential is also desirable as it may have an important role in low-temperature collisions and large impact parameters.[29] The interaction potential is characterized by a van der Waals dispersion well that has a depth dependent on the polarizability of the species, so that it is expected to increase for heavier inert gas atoms or charged targets. Here the interaction potential is determined by nonlinear least-squares fit of a set of parameters to several hundred of ab initio single energy calculations. Of the models previously used to describe the interaction potential, studies have demonstrated that modified Buckingam (exp-6) potentials in general outperform Lennard-Jones ones.[30,41] Here a more sophisticated representation is used and described in more detail in the next section.

The bottleneck to refining or extending computational approaches to complex molecules is represented by the increased complexity of the PES and, at the same time, the unknown reliability of the common model potentials used to approximate it. In any case, species of interest in chemical processes (for instance combustion) are not limited to only four or five atoms, and the study of energy transfer and related phenomena in large molecules is essentially still today an unexplored field. Radical species play a fundamental role in combustion and atmospheric chemistry and studies of collision-induced recombination of radicals are challenging in several respects. These challenges are well-illustrated by the relatively simple example of recombination of O_2 with O to make O_3 and subsequent stabilization in collisions with an inert collider, e.g., Ar.[43−46] These studies come close to the ideal description of examining collisions of the inert collider with the metastable incipient polyatomic. They are of course highly computationally demanding for a number of reasons, from the perspective of both the potentials and the dynamics. For the former the complete potential can be fruitfully divided into two parts. The first part is the potential for the radical−radical system. This must be known from the global minimum up to the asymptotic dissociation limit. The second component of the potential is the interaction with the "inert" collider. This intermolecular potential is of course of higher mathematical dimensionality than the molecular potential but for inert interactions it is of a much simpler form and so hopefully can be represented relatively simply. Although this research is still ongoing, global potentials for O_3 do exist as do simple, i.e., sum-of-pairs, semiempirical interaction potentials for the Ar−O_3 system.

The main novelties of the present paper lie in the choice of a relatively large radical, C_3H_5 (allyl), as the target molecule, the availability of an intramolecular potential which is a full-dimensional permutationally invariant PES[47] and an intermolecular potential able to accurately describe the interaction even for different allyl isomers. In the present paper, we are able to study energy transfer in a complex system without introducing approximations in the description of the intramolecular potential. For a polyatomic target (like allyl), the intramolecular potential may itself be extremely challenging to describe, but recently a technique[48,49] able to produce an analytical full-dimensional PES, invariant under permutation of atoms for systems made of 6−8 atoms has been developed. Moreover, in contrast to the case of molecules like CH_4 or CO_2 where a single stable minimum is present and a statistical distribution of initial conditions is direct, the full-dimensional allyl PES presents several energetically accessible isomers and, in a future perspective, a different way of sampling initial conditions may be considered. The interaction potential is itself reliable also for geometries distorted from the global minimum one. The work opens up the possibility for future investigation of the role of collisions on isomerizations and unimolecular dissociation branching ratios. In this paper, we use the initial conditions of previous full dimensional classical trajectory calculations of the unimolecular dissociation of allyl to several products.[50] The internal energy is set to be about 157 kcal/mol, of relevance to interesting and initially puzzling photodissociation experiments.[51,52]

As for highly efficient collisions, previous studies have shown that they may be determined by an impulsive, hard-sphere like V → T event in the presence of high relative translational energies,[53] or may be induced by formation of collision complexes[54] that favor randomization of energy between all

degrees of freedom.[55] One proposed definition to characterize an otherwise totally qualitative concept is to include in the ensemble of higly efficient collisions those with an energy transfer bigger than 5 times the average energy transfer down.[19] We will show that a biexponential fit of the energy transfer probability density identifies two regimes for collisions (weak and strong). The "5 times the average" metric,[19] even if somewhat arbitrary, defines a threshold energy in the tail of the strong collision regime, thus remaining an acceptable criterion for highly efficient collisions.

In this paper, we report an investigation of single argon collisions with vibrationally hot allyl radicals. Energy transfers from and to the allyl are considered for different values of the impact parameter and the collision energy. The full-dimensional PES is represented as the intramolecular potential of allyl plus an approximation to the interaction potential. For the 18-dimensional allyl intramolecular potential a permutationally invariant full-dimensional PES is available, which has already been employed for a quasiclassical study of allyl unimolecular dynamics and branching ratios.[50] The intermolecular potential is obtained here by a nonlinear minimum least-squares fit of 14 parameters to a set of almost 300 ab initio MP2/avtz counterpoise-corrected single-energy points. The availability of an accurate full-dimensional PES for the target, besides yielding more realistic and reliable results, allows for a classically exact description of the internal molecular motion and its perturbation during the scattering process. Three different thermal collision energies are considered, and the sensitivity of results to the intermolecular potential is tested.

THE INTERACTION POTENTIAL AND THE ALLYL PES

The allyl potential energy surface is a precise mathematical fit to 97 418 electronic energies at the CCSD(T)/aug-cc-pVTZ level of theory, as described in detail elsewhere.[47,50] The PES is quite rugged, as can be appreciated from the usual schematic plot given in Figure 1. As seen, there are numerous minima and

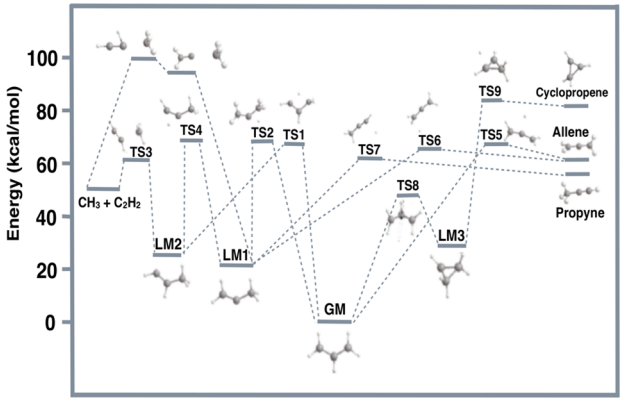

Figure 1. Schematic plot of the allyl PES.

saddle points separating them. The products of the dissociation of allyl and its isomers are also indicated. The corresponding energy values for local minima, transition states, and fragment channels are reported in Table 1 relative to the global minimum. In addition to the complexity indicated in this figure, the PES contains a further complexity due to the high degree of permutational symmetry of the 5 identical H atoms and the 3 identical C atoms; i.e., the total number of

Table 1. Energy Values of the Allyl PES Relative to the Global Minimum (kcal/mol)

stationary point	energy
GM	0
LM1	20.4
LM2	25.0
LM3	29.5
TS1	69.6
TS2	70.5
TS3	62.5
TS4	70.9
TS5	69.4
TS6	66.4
TS7	63.5
TS8	51.9
TS9	86.7
HCCH + CH_3	52.4
allene + H	62.9
propyne + H	58.4
cyclopropene + H	83.5

permutations is 5!3! = 720 and thus there are 719 additional equivalent structures indicated in Figure 1. The PES here employed obeys this full permutational invariance. The complexity of this molecular potential makes it attractive to us for the first studies of energy transfer for several reasons. First, it is actually typical of many polyatomic molecules that occur in combustion and atmospheric chemistry, with multiple minima and reaction channels. Second, from a fundamental point of view collisions with a molecule or an inert atom can lead to several outcomes of interest beyond simple energy transfer. For example, such collisions can induce isomerization or alter the reaction branching ratios. Even energy transfer is potentially complex as different isomers may show different energy transfer properties. All of these processes will be studied in a series of papers, beginning with this one, where the focus is on the interaction potential with Ar and energy transfer from the most stable form of C_3H_5, allyl.

The full-dimensional potential needed to study the argon−allyl collision process is described by means of the general expression

$$V_{Ar-C_3H_5} = V_{intra} + V_{inter} \quad (1)$$

where V_{intra} is the isolated allyl potential for which a permutationally invariant full-dimensional PES is available, and V_{inter} is the rare gas + C_3H_5 intermolecular potential approximated by a pairwise function dependent only on the Ar−H and Ar−C distances. Computational times are out of reach for direct-dynamics calculations. In fact, a single energy calculation (MP2/avtz) with MOLPRO on a single core takes about 10 min CPU time. MP2 analytic gradient calculations are even more expensive (of about a factor of 5), and a single trajectory consists on average of 15−20 thousands steps (depending on initial conditions), thus making direct-dynamics not feasible for the allyl−argon system at this level of ab initio theory.

The interaction potential was sampled at a total of 286 different configurations. Single-energy calculations were performed for different geometries of the allyl molecule, different distances of the argon atom from the center of mass of the target and different orientations of the allyl with respect to the incoming argon. Three different geometries were

considered for the allyl, which are indicated as GM (142 ab initio points), LM1(71 ab initio points), and LM2 (73 ab initio points) in ref 50. With the allyl in the GM planar geometry, three potential cuts were chosen at different orientations, all of them directed toward the center of mass. The orientations were (1) perpendicular to the plane, (2) in the plane but opposite the central CH bond, and (3) halfway between the previous two cuts, i.e., at 45° with respect to the molecular plane. The distance along the cuts ranged from about 2 to around 7 Å to describe both the repulsive wall of the interaction potential and the van der Waals well. Points were sampled more densely near the bottom of the well. The MP2 level of theory was chosen for the ab initio calculations and the aug-cc-pvtz (avtz) basis set employed. In Figure 2 a cut is reported with energies for both

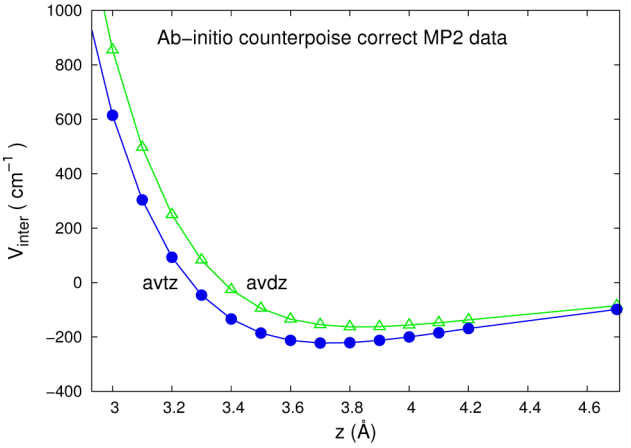

Figure 2. Ab initio counterpoise correct MP2 points for the avdz (green triangles) and avtz (blue dots) basis sets. The allyl is in the GM geometry and the orientation of the cut is perpendicular to the molecular plane.

aug-cc-pvdz (avdz) and bigger avtz basis sets. In a system made of two interacting species, like the one here under examination, the basis set superposition error (BSSE) consists of an artificial stabilization of the two-body complex due to the possibility for each monomer to use extra functions from the basis set of the other one at short distances. When the monomers are far apart from one another, instead, the basis sets do not overlap and the effect is not present. The result is an artificially deeper interaction well and a shorter equilibrium distance. To correct for BSSE, the electronic energies were counterpoise corrected according to the Boys and Bernardi scheme.[56] The correction is obtained by recalculating for each of the two species the isolated energy in a basis that includes also the functions of the other monomer but neglecting its electrons and nuclei.

The interaction potential was fit using the potential described by Varandas and Rodrigues.[57] The potential as a function of the distance R between the Ar and each type of atom in the allyl, H or C, is described by[58]

$$V_{Ar\beta}(R) = \lambda_{Ar\beta} V_{HF,\beta}(R) + V_{dc,\beta}(R) \qquad \beta = \text{H, C} \tag{2}$$

$$V_{HF}(R) = A\exp(-bR) \qquad V_{dc}(R) = -\sum \chi_n(R)\frac{C_n}{R_n}$$

$$n = 6, 8, 10 \tag{3}$$

These functions referred to in eq 3 are given explicitly by eqs 8−11 of ref 57. The equations contain 7 parameters for the potential between the Ar and each type of allyl atom, H, or C. The 286 potential energy points were fit in Mathematica[59] using the FindFit function with the "Gradient" method. Two fits were used in this work. The fit determined by the method above, which we call IntPES1, was saved and used for a sensitivity analysis, but this fit was not conclusively the best, because the machine precision was insufficient for the accuracy needed. This set of parameters did not fit the attractive portion of the potential energy cuts very well. The multidimensional surface of least-squares has many local minima, all of which have about the same depth. Thus, a manual search starting from the original parameters was undertaken using a plot of calculated vs fit potential points as a guide. This fit, named IntPES2, was one that gave about the same quality of overall fit, while fitting the attractive parts of the potential best. IntPES2 had an R^2 of 0.9925, and the RMS error varied from 22 cm^{-1} for the attractive region, to 150 cm^{-1} for energies around 1200 cm^{-1}, to 650 cm^{-1} for energies above 8000 cm^{-1}. The 14 parameters for the IntPES2 Ar-allyl fit, which was the one employed in the main simulations, are shown in Table 2.

Table 2. Parameters Adopted for the Interaction Potentials

	IntPES1		IntPES2	
parameter	C	H	C	H
C_6	0.168	19.968	30.05	19.95
C_8	1174.0	426.0	1174.0	426.0
C_{10}	26512.0	12300.0	26512.0	12300.0
R_0	7.786	7.100	7.308	7.273
A	29.091	61.939	8.123	4.033
b	1.936	1.606	1.696	1.696
λ	5.914	0.112	7.621	2.298

Another approach has been described by Pirani et al.[60] In this method, the potential is a function of the distance between the Ar atom and the location of each allyl bond, with the dependence described by a modified $[n(x), 6]$ function, as suggested by Maitland and Smith.[61] The modification is to make the well depth parameter and the distance at the minimum energy dependent on the angle between the argon and the bond. This approach was used to fit the potential energy points by allowing the parallel and perpendicular limits for the well depth parameter and the distance at minimum energy to vary, along with the parameters m and b from eqs 2 and 3 of ref 60.

The fits of the potential from Pirani et al.[60] to the calculated potential energy points were not nearly as good as those obtained using the approach by Varandas and Rodrigues.[57] To simplify the calculation of the angle between the Ar and each bond, the fit was performed for a subset of 142 points corresponding to the allyl geometry of the global minimum. The best fit, determined using Mathematica in a method similar to that described above, had an R^2 of 0.962. The RMS error varied from 131 cm^{-1} for the attractive region, to 492 cm^{-1} for energies around 1200 cm^{-1} to 1400 cm^{-1} for regions above 8000 cm^{-1}. In addition to providing a less accurate fit, the potential of Pirani et al. requires calculation of the angle between the argon and each bond. The computational overhead for this step can be large, particularly if, as a result of the collision, the allyl has a structure in which the bonding is not obvious.

Several cuts through the Ar−allyl potential energy surface are shown in Figure 3 to compare the calculated values with the fit

dx.doi.org/10.1021/jp410315r | J. Phys. Chem. A 2013, 117, 14028−14041

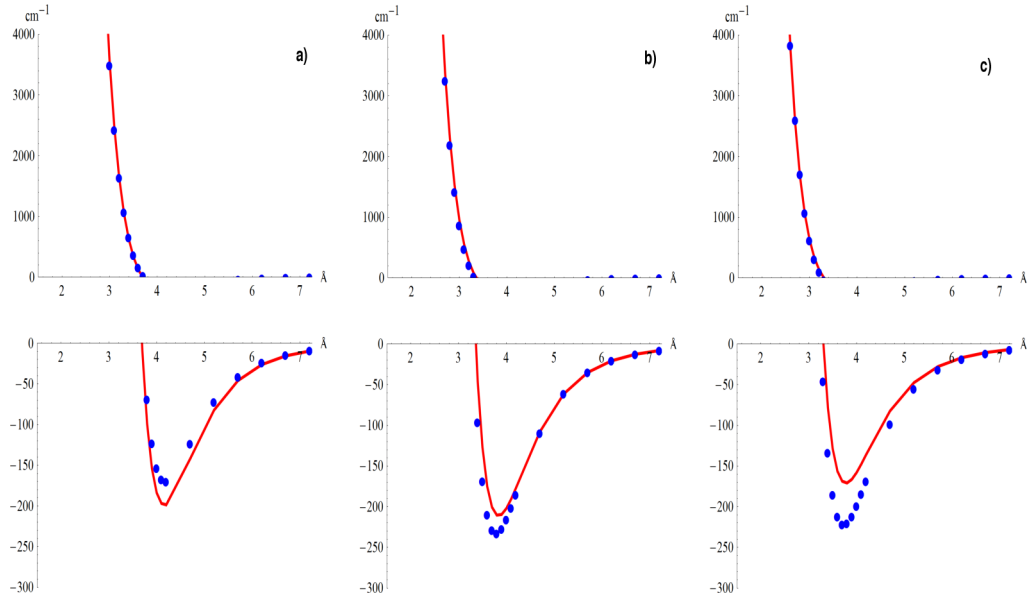

Figure 3. Comparisons between ab initio MP2/avtz counterpoise correct energies (blue dots) and the corresponding IntPES2 potential values (red solid line) for 3 potential cuts. (a) Potential cut in the molecular plane. (b) Potential cut at 45°. (c) Potential cut along a direction perpendicular to the molecular plane. The allyl is in the GM geometry.

based on the Varandas and Rodrigues approach. In general, the fit to the repulsive part of the potential is excellent, whereas the fit to the attractive part is good but not perfect. Fortunately, the calculated results are not very dependent on the attractive part, as discussed in the next section. Figure 4 shows a contour plot of the calculated interaction potential for approaches in the plane of the allyl molecule (upper) and in a plane containing the long axis of the allyl and the axis perpendicular to the plane of the allyl (bottom). Because it leaves out any multibody effects, the Varandas and Rodrigues approach is clearly oversimplified, but it has the virtue of being computationally efficient, simple, and sufficiently accurate for many purposes.

Furthermore, because the analytical interaction potential was fitted to a series of ab initio points mainly calculated with the allyl in the GM geometry, a potential cut was performed also for the molecule in the LM1 geometry to roughly evaluate the accuracy of the potential for geometries different from the global minimum one. Sixteen additional MP2/avtz counterpoise correct points were calculated on the plane, along a direction through the center of mass and equidistant from the two out-of-plane hydrogen atoms of the LM1 geometry. Figure 5 shows that the potential is accurate also in this case, thus making promising future studies involving isomerization processes or calculation of branching ratios possible.

DYNAMICS CALCULATIONS

To simulate collisions, initial conditions must be chosen for both allyl and argon. In a manner similar to that used in a previous paper,[50] we fixed the total internal energy of the molecule (E_0) to 55 000 cm^{-1} (at this energy allyl can dissociate to the products indicated in Figure 1). The microcanonical sampling was then performed by scaling of randomly chosen initial velocities for each atom of the molecule. The molecule, which had initially no angular momentum, was set in the GM geometry and given a random orientation by means of rotation through Euler angles. The argon atom and the target were initially separated by a distance of 15 au, which is big enough to avoid significant intermolecular

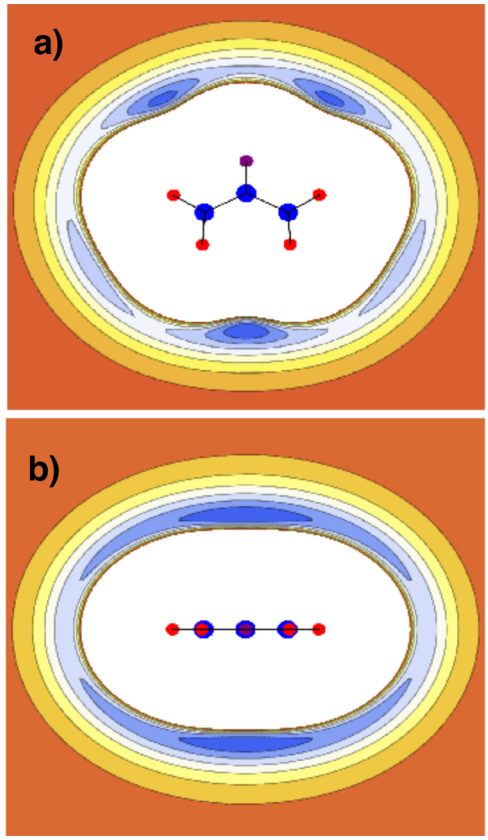

Figure 4. Contour plot of the argon−allyl potential. The darkest blue regions have the most attractive potential, whereas the red color shows the location of zero potential. The contours are spaced by 25 cm^{-1}. Panel a shows the potential for approaches in the plane of the allyl molecule. Panel b shows the potential for approaches in a plane containing the long axis of the allyl and the axis perpendicular to the plane of the allyl.

interaction. The whole system was finally rotated in such a way that Ar and the molecular center of mass were initially in the *xy*

dx.doi.org/10.1021/jp410315r | J. Phys. Chem. A 2013, 117, 14028−14041

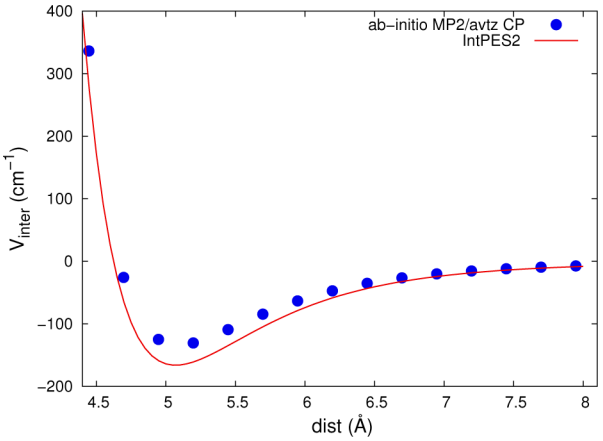

Figure 5. Ab initio MP2/avtz counterpoise corrected points (blue dots) and IntPES2 approximation (red solid line) for a potential cut with allyl in LM1 geometry. Points are sampled along a direction through the center of mass and equidistant from the two out-of-plane hydrogen atoms.

plane, with velocities pointing toward each other along the x direction. Consequently, the difference in the y coordinates corresponded to the impact parameter. The global center of mass was chosen at the origin of the Cartesian coordinates and given null velocity, so that by law of linear momentum conservation it was a fixed point during the complete collisional event. Simulations were performed for three different values of the collision energy: 0.3, 1.0, and 2.0 kcal/mol. From the collision energy one may easily determine the values of initial translational velocities for both Ar and allyl. In fact,

$$\mathbf{P}_{tot} = m_{Ar}\mathbf{v}_{Ar} + m_{mol}\mathbf{v}_{mol} = \mathbf{0} \quad (4)$$

$$E_{coll} = P_r^2/2\mu \qquad P_r = m_{Ar}v_{Ar} = m_{mol}v_{mol} \quad (5)$$

From eq 4 it may be inferred that the ratio between translational kinetic energies of the collider and the molecule is a constant of motion (the constant equals m_{mol}/m_{Ar} = 1.0273) and it was indeed used together with total energy, total angular momentum, and position of the global center of mass conservations as a check for numerical consistency of the simulations. Trajectories were classically evolved adopting a velocity-Verlet integration algorithm and a time step of 0.1 fs. The impact parameter, b, was scanned from 0 to b_{max} with a step size of 0.5 au. The total energy was typically conserved along trajectories with an accuracy of 1 part in 10^4. For each value of b, 500 trajectories were calculated.

The value of b_{max} cannot be uniquely defined for a process not involving complex-forming or reactive trajectories because energy transfer approaches 0 only asymptotically. Thus, in the choice of the best maximum impact parameter there is a trade-off between the necessity to include all significant energy-transfer events and the desire to avoid the effort of following uninteresting encounters. We did not choose to use some of the criteria employed in previous research in the field, for example, that based on convergence of second momenta of rate coefficients[41] or that based on a definition of b_{max} as the minimum impact parameter value for which no trajectory in a batch of 50 runs shows 3 or more turning points.[35] Instead, we looked at the cumulative total energy transfer and determined b_{max} as the value where the curve becomes almost flat,[62] indicating that further contributions for larger values of b can be neglected as they are smaller and smaller. To better check the accuracy of the b_{max} value chosen, we have additionally

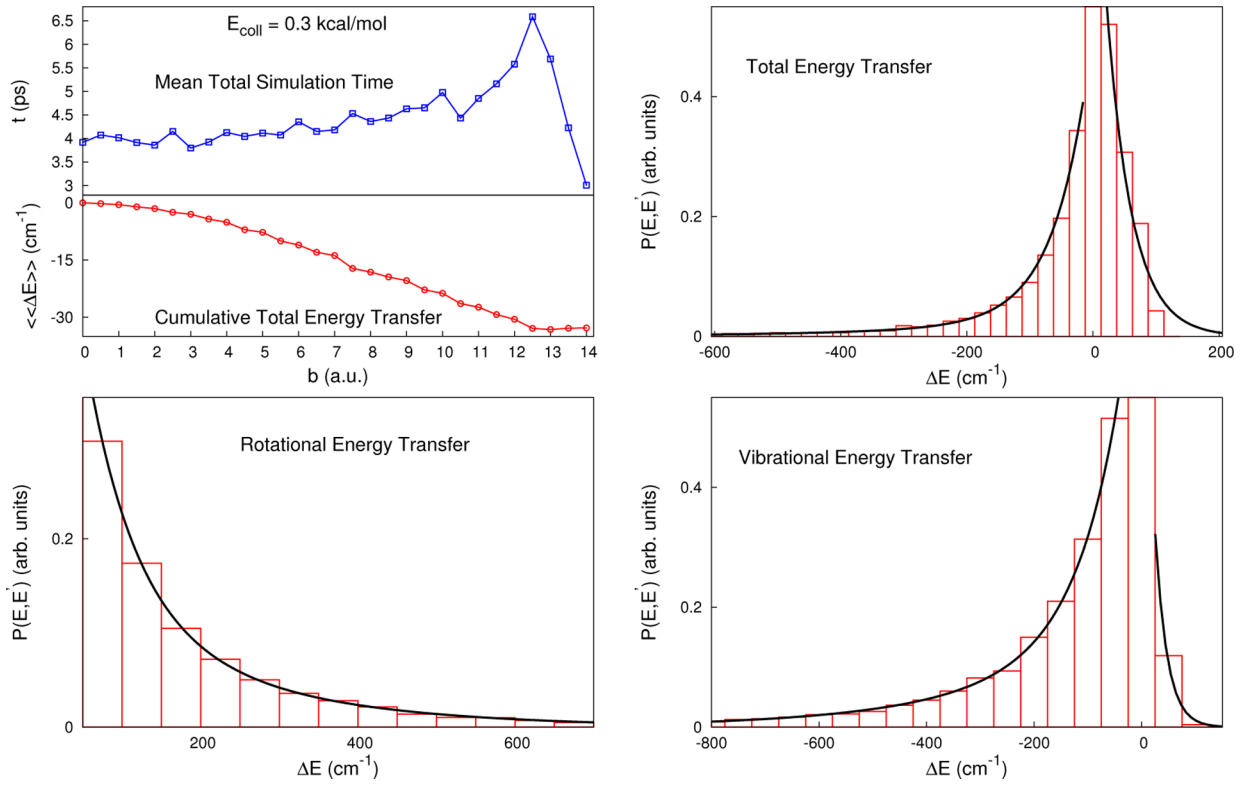

Figure 6. Mean total simulation time, cumulative total energy transfer, and histograms for average total, rotational, and vibrational energy transfers at E_{coll} = 0.3 kcal/mol. The zero bin is excluded in the fit.

dx.doi.org/10.1021/jp410315r | J. Phys. Chem. A 2013, 117, 14028−14041

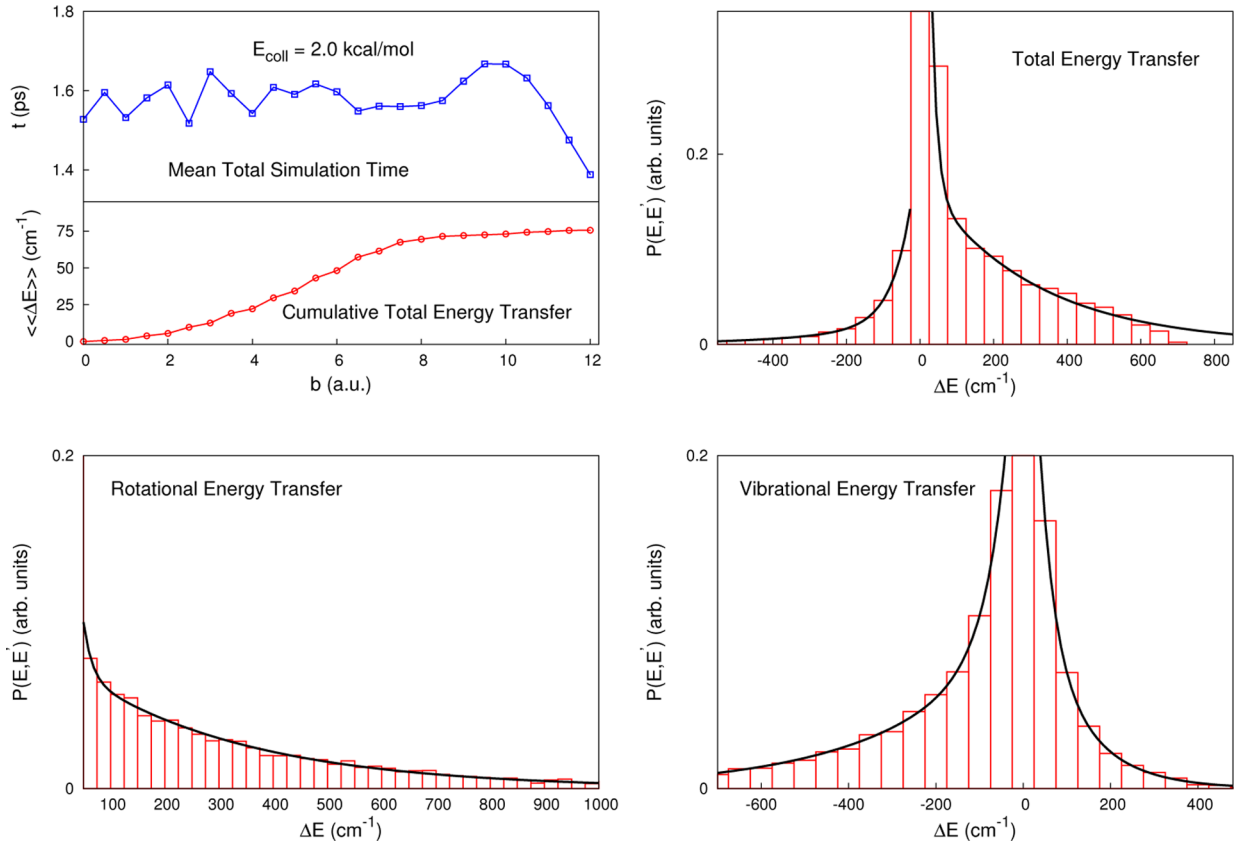

Figure 7. Mean total simulation time, cumulative total energy transfer, and histograms for average total, rotational, and vibrational energy transfers at E_{coll} = 2.0 kcal/mol. The zero bin is excluded in the fit.

considered the mean total simulation time. This is expected to drop steeply when the desired value of b_{max} is reached, because interaction is almost negligible and the total simulation time eventually converges to the simulation time of noninteracting particles.[54]

The outcome of each run of trajectories could be divided into two groups. One group consisted of trajectories that completed the whole scattering process and were stopped when the distance between the rare gas atom and the nearest of allyl atoms was bigger than 16 au. The other group consisted of trajectories that could not terminate because of dissociation of the allyl. A trajectory was stopped if at least one of the distances between the allyl atoms was greater than 20 au. Trajectories belonging to this second group were discarded and not considered in the energy transfer analysis.

Plots of the main results are shown in Figure 6 and Figure 7 for E_{coll} = 0.3 kcal/mol and E_{coll} = 2.0 kcal/mol, respectively. In the upper left panel, two b-dependent quantities are plotted. On the bottom half of this panel, the b-dependent cumulative total energy transfer is shown. It is defined by[62]

$$\langle\langle \Delta E^{tot}\rangle\rangle(E_{coll},b) = \frac{2}{b^2}\int_0^b db'\, b'\langle \Delta E^{tot}(E_{coll},b')\rangle \qquad (6)$$

The b-dependent single averages in the integrand were calculated for each impact parameter from the subset of trajectories that completed the whole scattering process without being prematurely aborted due to the breaking of any molecular bond. The cumulative total energy transfer, indicated on the left-hand side of eq 6 as a double average, is obtained as an integral average limited to the b value considered. When b equals b_{max}, eq 6 defines the average total energy transfer ($\langle\langle \Delta E^{tot}\rangle\rangle$) for the particular collision energy under examination. The integration in eq 6 was performed by numerical quadrature with a step size of 0.5 au and employing an extended three-point Newton−Cotes scheme. On the upper half of the same panel, the previously discussed mean total simulation time is reported as a function of b. It is as well calculated as an ensemble average from complete trajectories. The peak in simulation time before b_{max} can be interpreted as corresponding to the value of impact parameter at which orbiting occurs and the collision lifetime is a maximum.[54]

The remaining panels in Figures 6 and 7 reproduce histograms for three different types of energy transfers. The change in the rotational energy for the ith trajectory is defined as

$$\Delta E_i^{rot} = \frac{1}{2} I_i \omega_i^2 \qquad (7)$$

I_i and ω_i are determined going to the principal axes frame, where the inertia tensor is diagonal, calculating the angular momentum and deriving ω_i by inversion of the (diagonal) inertia tensor. The change in vibrational energy, instead, is calculated by difference as $\Delta E_i^{vib} = (\Delta E_i^{tot} - \Delta E_i^{rot})$.

Starting from the upper right one and moving clockwise, the panels present histograms for the total, vibrational, and rotational energy transfers, respectively. The histograms were obtained after calculation of the different energy transfers for each complete trajectory. The binning was done assigning every energy transfer a weight equal to the impact parameter of the corresponding trajectory. The bin width is usually 50

dx.doi.org/10.1021/jp410315r | J. Phys. Chem. A 2013, 117, 14028−14041

wavenumbers with a few exceptions, for which a width of 25 cm^{-1} was chosen to feature the details of the distribution around 0. The final relative probability distribution P(E,E′) was obtained by scaling to 1 the value of the central bin. However, the number of trajectories landing in the zero bin is arbitrary and depends on the choice of b_{max}. The heights of the other bins relative to each other, instead, are well-defined and allow comparisons. For this reason, we choose to plot histograms excluding the central bin and yielding a better representation of all the other bins.

A comparison between results at different collision energies shows, first, that most collision events yield small energy transfers, independent of the relative velocity. Nearly elastic scattering is the most frequent event, and the histograms show exponential-like decays, so events involving huge energies are rare. Second, an increment in relative energy shifts histograms to more positive energies, reflecting the fact that collision energy acts as an upper bound to positive energy transfer.

To check the reliability of the results previously presented, their sensitivity to a parametrical change in the potential was tested. Figure 8 reports the perpendicular potential cut

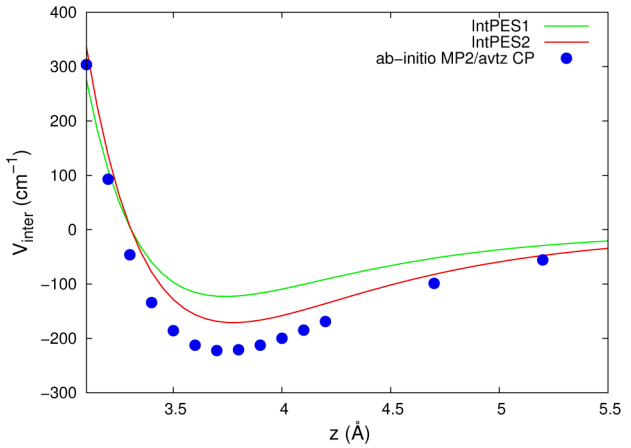

Figure 8. Comparison of potential cut energies between IntPES2 (red), IntPES1 (green), and ab initio MP2/avtz counterpoise correct data (blue dots). The cut is chosen perpendicular to the molecular plane with allyl in GM geometry.

obtained with IntPES1 and intPES2 potentials. As one may see, IntPES1 deviates from IntPES2 and gives a worse approximation especially in the attractive region. As already stated in the Introduction, the accuracy of the main features of a collision simulation depends mostly on the ability to describe the hardness of the repulsive wall. It was of primary interest for us to explore how our results were affected by the diminished accuracy of IntPES1.

Figures 9 and 10 show energy transfers and other quantities for the two different fit potentials. The sensitivity test was performed using IntPES1, starting trajectories from exactly the same initial conditions adopted for the runs at E_{coll} = 1 kcal/mol with IntPES2. Thus, if trajectories evolve somehow differently and final outcomes are not substantially similar, the effect is determined uniquely by the different kind of fit potential employed. Comparison of the two figures reveals that only minor differences can be discerned. The shape of histograms is quite remarkably maintained, whereas data reported in Table 3 demonstrate that the value of the total energy transfer is slightly reduced for the sensitivity test (IntPES1 potential) and so are vibrational and rotational energy transfers, with the most significant difference in the latter. This is in agreement with a reduced mean total simulation time that is attributable to a reduction of the pure interaction time (i.e., the fraction of the total simulation which is due to the actual interaction between argon and allyl). Another way to explain the slightly quenched energy transfers is to consider IntPES1 as the one describing less accurately the interaction region. This is actually consistent with the potential cut shown in Figure 8. The outcome of the sensitivity test allows us to conclude that the system did not experience dramatic changes in energy transfer processes when the analytical interaction potential was modified even significantly in some regions (Figure 8). This is an important feature for the reliability of our present results and for future work. On one hand, weak sensitivity of results means that a further refinement of the fit interaction potential is not really necessary, especially if it would neccessitate accounting for three-body or higher order interactions. On the other hand, applications involving different geometries of the allyl are encouraged, because IntPES2 appears to be accurate enough even for geometries other than the global minimum one (see the LM1 potential cut in Figure 5).

We present a summary of relevant data in Table 3. Simulation results are reported for three different collision energies and for the sensitivity test (column 1). Looking at column 2 with the values of maximum impact parameter, it is possible to identify a decreasing trend in b_{max} with increasing collision energy. This is an anticipated result, because at lower relative energies motion can be perturbed by lower interaction energies. The various per-collision average energy transfer values (presented in columns 3−5) were obtained from eq 6 at $b = b_{max}$. These average values, calculated from trajectory simulations, are referenced to the hard sphere collision rate (Z_{HS}) evaluated at b_{max}[29]

$$Z_{HS} = \pi b_{max}^2 \sqrt{8k_B T_{bath}/\pi\mu} \tag{8}$$

μ is the argon−allyl reduced mass. In our system, the collision energies correspond to the mean translational energies related to the temperature of the bath by $E_{coll} = 2k_B T_{bath}$[55,65] and can be used to determine the average energy transfer rate[29]

$$r_{\Delta E} = Z_{HS}\langle \Delta E \rangle \tag{9}$$

This is the observable that is not dependent on the b_{max} value chosen (provided it is large enough to include all sizable energy transfers) or on the collision rate.

Column 3 shows that increasing the relative kinetic energy enhances the rotational energy transfer, which can only be positive because, initially, the allyl was given no angular momentum. Differently from rotational energy, we found that allyl is vibrationally quenched by collisions at all energies (column 4). The vibrational relaxation process implies also observation of highly efficient collisions, which we treat in more detail in the last part of this section. In column 5, the average total energy transfer is reported. It changes sign moving from E_{coll} = 0.3 kcal/mol to E_{coll} = 1.0 kcal/mol and it further increases with relative energy. So, if at the lowest collision energy the molecule is stabilized, at higher energies allyl is further excited. This additional excitation is entirely stored in the rotational motion as can be derived from the negative average vibrational energy values of column 4. Column 6 lists the values of the hard sphere collision rates at different collision

dx.doi.org/10.1021/jp410315r | J. Phys. Chem. A 2013, 117, 14028−14041

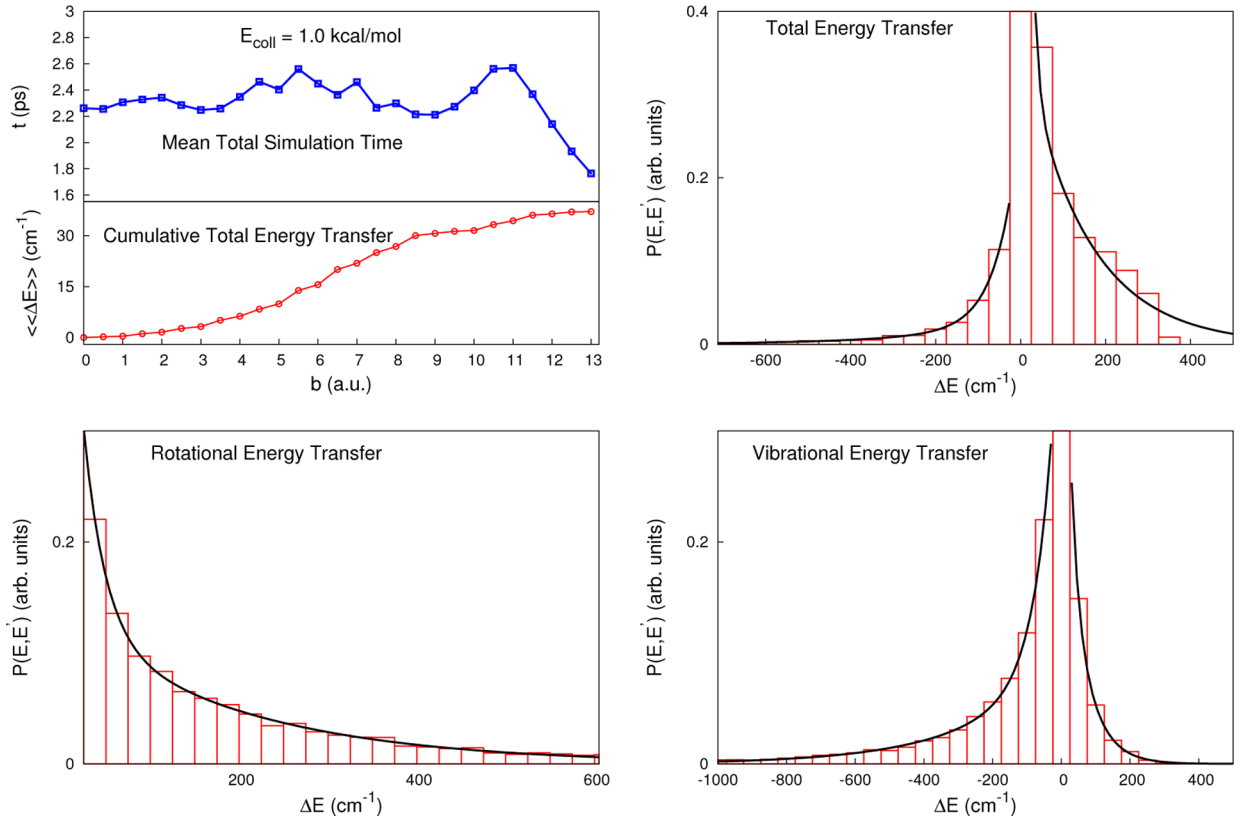

Figure 9. Mean total simulation time, cumulative total energy transfer, and histograms for average total, rotational, and vibrational energy transfers at E_{coll} = 1.0 kcal/mol. The IntPES2 interaction potential is employed. The zero bin is excluded in the fit.

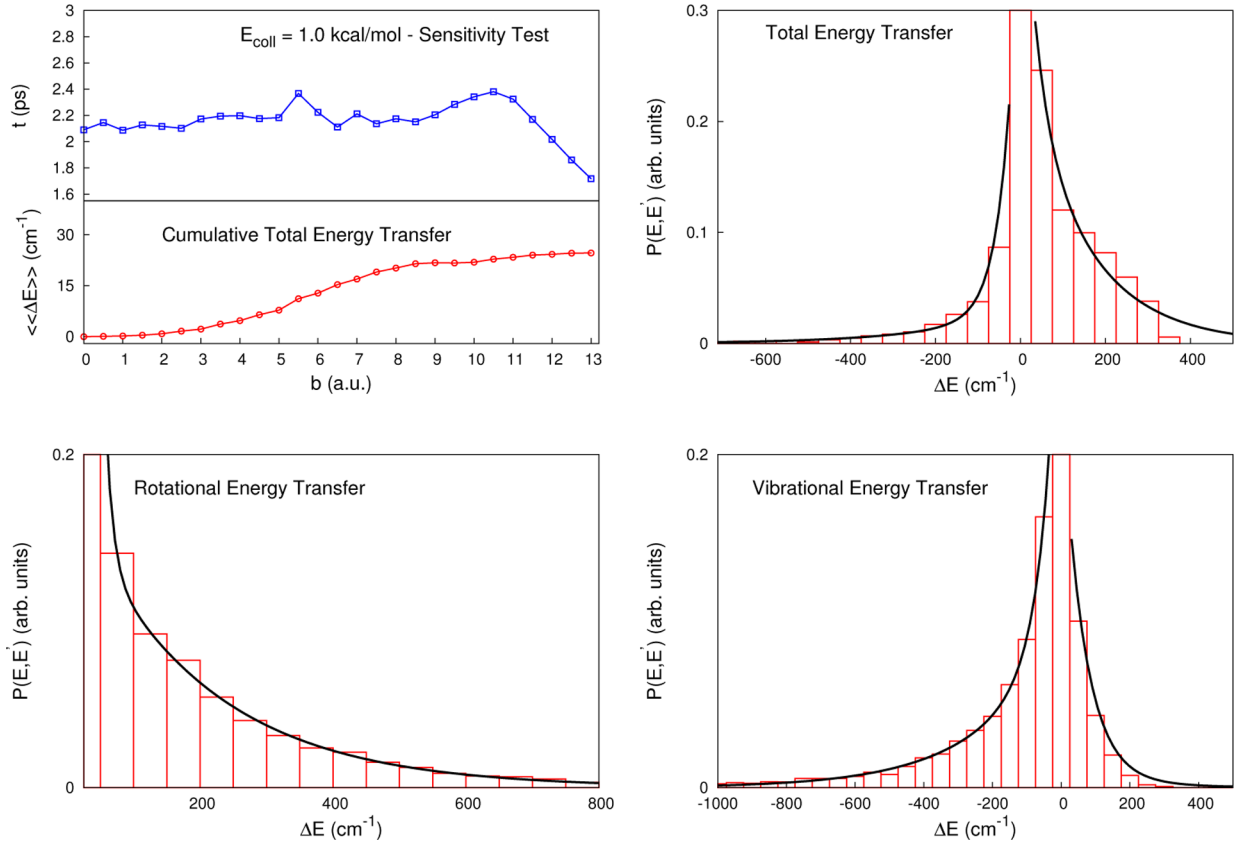

Figure 10. Mean total simulation time, cumulative total energy transfer, and histograms for average total, rotational, and vibrational energy tranfers at E_{coll} = 1.0 kcal/mol. This sensitivity test uses the IntPES1 interaction potential. The zero bin is excluded in the fit.

dx.doi.org/10.1021/jp410315r | J. Phys. Chem. A 2013, 117, 14028−14041

Table 3. Collision Energy, Maximum Impact Parameter, Average Rotational, Vibrational and Total Energy Transfers, Maximum Value for Rotational Energy Transfer, and Fraction of Complete Collisions (Allyl Internal Excitation E_0 = 55 000 cm^{-1})

E_{coll}[a]	b_{max}[b]	$\langle\langle\Delta E^{rot}\rangle\rangle$[c]	$\langle\langle\Delta E^{vib}\rangle\rangle$[c]	$\langle\langle\Delta E^{tot}\rangle\rangle$[c]	Z_{HS}[d]	$r_{\Delta E_{tot}}$[e]	complete trajs %
0.3	14.0	112.93	−145.70	−32.77	4.84	−158.61	74.03
1.0	13.0	126.41	−89.33	37.08	7.63	282.92	88.63
1.0 (Sens)	13.0	106.02	−81.37	24.65	7.63	188.08	89.47
2.0	12.0	180.60	−104.96	75.65	9.19	695.22	92.51

[a]kcal/mol. [b]au. [c]cm^{-1}. [d]10^{-10} cm^3 $molecule^{-1}$ s^{-1}. [e]10^{-10} cm^{-1} cm^3 s^{-1}.

Table 4. Fit Parameters for the Total Energy Transfer Histograms, Crossover Energy from "Weak" to "Strong" Regime, and Highly Efficient Collision Threshold Energy

E_{coll}[a]	a	b	c	d	a'	b'	c'	d'	crossover[b]	HEC threshold[b]
0.3	250.05	55.08	0.035	0.478	39.97	2.64	0.95	0.15	−184	−518
1.0	239.00	50.61	0.028	0.245	148.16	11.12	0.368	2.41	−139	−425
1.0 (Sens)	215.50	35.05	0.032	0.40	148.15	34.27	0.252	0.249	−110	−431
2.0	262.30	51.29	0.028	0.199	302.90	15.60	0.175	1.55	−124	−609

[a]kcal/mol. [b]cm^{-1}.

energies. The values increase with the collision energy or, equivalently, the temperature of the bath. In column 7 the average total energy transfer rates are reported. These values permit a more straightforward comparison at different collision energies, because they account for different hard sphere collision rates. The trend already pointed out by column 5 is confirmed, but the increase in energy transfer for the highest collision energy appears now to be steeper. Finally, in column 8, the fraction of complete trajectories is reported. Complete trajectories are those which exit the simulation according to the criterion previously described without any bond breaking happening. The percentage of complete trajectories increases with relative energy because the collision process is faster and then less time is available to the molecule for breaking a bond.

Transition probability densities $P(E,E')$ reported in the histograms were fitted. Biexponential functions have been adopted to show the exponential decay of probabilities with energy transfer. Analytic expressions for the probabilities were chosen similarly to previous work in the field.[63] The "up" and "down" wings of the energy transfer distribution are fitted separately and the central bin is excluded.

$$P(E,E') = c\exp(-z/a) + d\exp(-z/b) \qquad z = |E' - E| \tag{10}$$

Table 4 reports the parameters of our histogram fits for the average total energy transfer. Parameters relative to the "up" wing are primed (a', b', c', d'). c and d are the "weight" parameters, and a and b are the "exponential" parameters that characterize (following Troe's terminology[64]), respectively, the "strong" and "weak" components of the energy transfer. "Strong" exponential parameters are about 5 times bigger than the corresponding "weak" ones. For the "down" wing, Figure 11 shows on the upper half the fitted total energy transfer histogram relative to the 0.3 kcal/mol collision energy, whereas on the lower half the corresponding semilog plot is reported. The two straight lines on the semilog plot identifies the two exponentials and so the two collisional regimes, roughly separated at the energy indicated by the crossover point where the two lines intersect. A different estimate of the crossover energy might be obtained by fitting separately the weak regime directly on the semilog plot. The two estimates differ by about 100 wavenumbers, thus identifying a crossover range. However, from data in Table 4 it is clear that the threshold energy obtained on the basis of Clary's "5 times the average" metric is positioned farther in the tail of the strong collision regime, thus validating the practical criterion we adopt to determine highly efficient collisions.

In our simulations, a restricted subset of trajectories was characterized by a large amount of V → T energy transfer if compared to the average energy transfer down. As stated before, a practical way (validated for our system) to define highly efficient collisions is to look at collisions with an energy transfer that is at least 5 times the average energy down.[19] Table 5 reports the principal data about HEC found in our simulations. For different collision energies (column 1), column 2 shows the average energy transfer down that is calculated averaging only over collisions that relax the molecule. Columns 3 and 4, instead, are related to the fraction of HEC among all trajectories. We report both the simple unweighted ratio (column 3) and the b-weighted one (column 4). Interestingly, the weighted values are smaller than the unweighted ones, indicating that HEC appears to be privileged at smaller impact parameters. Furthermore, the percentage of highly efficient collisions is decreasing for increasing values of collision energy. Column 5 indicates that, in agreement with the weighted ratio, HEC has a bigger impact on the average total energy transfer at lower relative energy. However, the trend is inverted when looking at how highly efficient collisions influence the average energy transfer down (column 6). As previously stated, the average transfer energy down is calculated in the subset of trajectories with negative energy transfer, so it is useful to examine the percentage of HEC restricted to this subset (last column). What we found is that this fraction is significantly smaller at E_{coll} = 0.3 kcal/mol, thus explaining the minor importance of HEC to the average energy down.

Large energy transfers are rare events and consequently are expected to be particularly sensitive to a change in the interaction potential parameters. This is exactly what is reported by data in Table 5. Sensitivity simulations are shown to give similar results for average energy down, but appreciably different ones when HEC values or HEC influence on average data are considered. The difference probably arises from a different approximation of the repulsive wall. Figure 12 presents histograms of the b-weighted distributions restricted to highly efficient collisions only. The histograms have an upper bound due to the 5-time average energy transfer down requirement

dx.doi.org/10.1021/jp410315r | J. Phys. Chem. A 2013, 117, 14028−14041

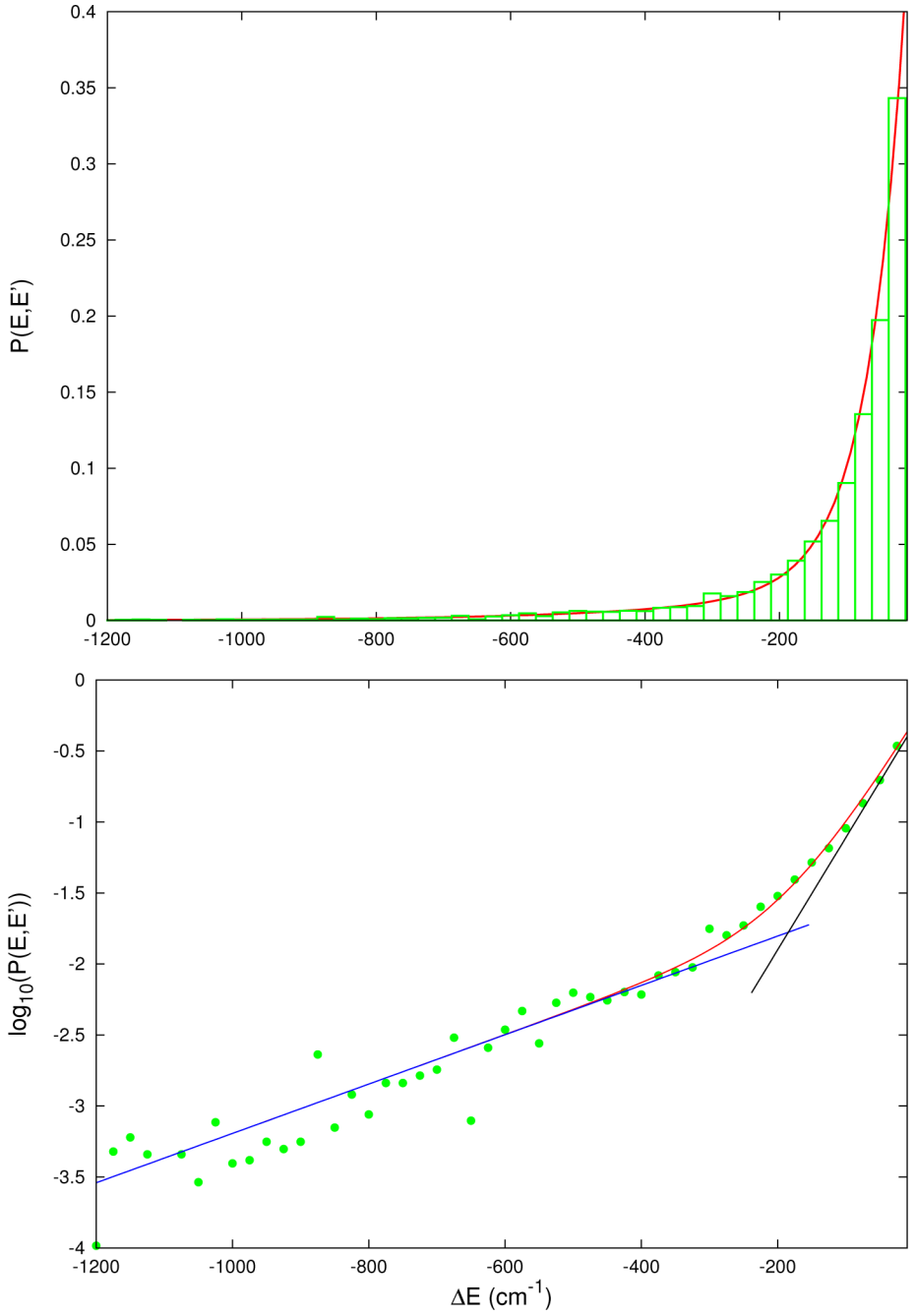

Figure 11. Histogram and semilog plots for the average total energy transfer at collision energy 0.3 kcal/mol.

Table 5. Collision Energy, Average Energy Down, HEC Fraction, HEC *b*-weighted Fraction, Relative Weight of HEC on Average Total Energy, Fraction of Average Energy Down Due to HEC, and Fraction of HEC Among Energy Down Collisions (Allyl Internal Excitation E_0 = 55 000 cm^{-1})

E_{coll} [a]	$\langle\langle \Delta E^{down} \rangle\rangle$ [b]	% HEC	% HEC (b-w)	% $\langle\langle \Delta E^{tot} \rangle\rangle$	% $\langle\langle \Delta E^{down} \rangle\rangle$	% n_{HEC}/n_{down}
0.3	−103.62	2.18	1.40	37.0	23.4	4.72
1.0	−85.02	2.40	1.15	21.2	33.2	10.02
1.0 (Sens)	−86.17	2.39	1.09	38.3	39.8	8.99
2.0	−121.87	1.91	0.91	13.5	39.5	8.48

[a]kcal/mol. [b]cm^{-1}.

and the bin width is chosen equal to $\langle\langle \Delta E^{down} \rangle\rangle$. Sensitivity results appear to show more differences near the threshold limit. The relative population of large energy transfers is enhanced at higher collision energy. The majority of highly efficient collisions are characterized by trajectories that terminate fast, with a single turning point and a total simulation time well under the typical scale time reported in previous histogram panels. Total simulation time decreases with relative

dx.doi.org/10.1021/jp410315r | J. Phys. Chem. A 2013, 117, 14028−14041

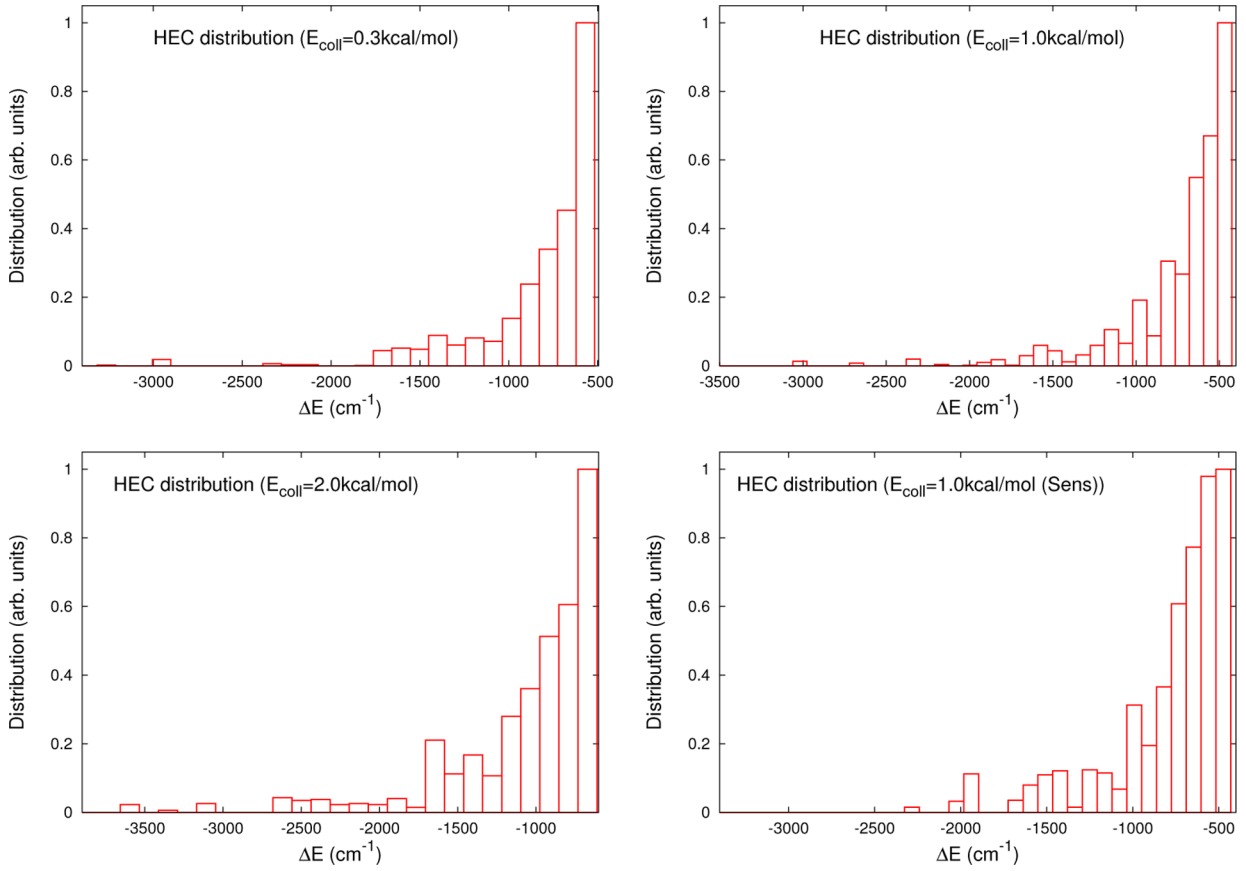

Figure 12. Highly efficient collision distributions at different collision energies.

energy. On the other hand, a few HEC feature long-time trajectories with several turning points with the argon atom hovering above the allyl before undergoing the final collision. This type of "slow" HEC is more common at E_{coll} = 0.3 kcal/mol and much less frequent for higher collision energies. Animations of highly efficient collisions show that they take place when a hydrogen atom comes close to the argon, after some bending, stretch, or torsion motion of the allyl. The hydrogen atom involved in the HEC can be the central one of the allyl or one of the hydrogens in the terminal $-CH_2$ groups. The Ar−H distance can be smaller than 2 Å, especially when the impact parameter is small. The interaction potential goes up along the repulsive wall, and the energy is then impulsively transferred to the translational motion. Finally, we can state in agreement with ref 19 that also in our allyl−argon system highly efficient collisions are found at different collision energies and have different duration. In our calculations we found a predominance of HEC for low impact parameters, corresponding to predominant backward HEC scattering, a phenomenon that has been experimentally observed for instance in the azulene−krypton system of ref 17.

SUMMARY AND CONCLUSIONS

In this first paper we have presented classical scattering simulations for the allyl−argon system. The work has been mainly focused on the determination of the interaction potential and the study of energy transfer processes. The results are quite satisfactory. The interaction potential is dependent just on two-body interactions through Ar−C and Ar−H distances. Only 14 nonlinear parameters have been fit to a limited set of ab initio points. The interaction potential has been demonstrated to be accurate also for allyl geometries different from the global minimum one. Energy transfer results describe efficiently the physics of inelastic scattering collisions. Highly efficient collisions have been detected and investigated. The union of a permutationally invariant PES for allyl with an effective interaction potential certifies the reliability of the results presented and encourages further and more detailed work. Among the topics that could be of interest in future research are how the energy transfer depends on the allyl isomer, how isomerization or dissociation is induced by collisions, and whether product branching ratios depend on collisional parameters.

AUTHOR INFORMATION

Corresponding Authors

*R. Conte: e-mail, riccardo.conte@emory.edu.
*P. L. Houston: e-mail, paul.houston@cos.gatech.edu.
*J. M. Bowman: e-mail, jmbowma@emory.edu.

Notes

The authors declare no competing financial interest.

ACKNOWLEDGMENTS

R.C. and J.M.B. thank the Department of Energy (DE-FG02-97ER14782) for support.

REFERENCES

(1) Löhmannsröben, H. L.; Luther, K. Selective Multiphoton Ionization in Dense Manifolds of Vibrational States. *Chem. Phys. Lett.* **1988**, *144*, 473−478.
(2) Mullin, A. S.; Michaels, C. A.; Flynn, G. W. Molecular Supercollisions: Evidence for Large Energy Transfer in the Collisional

Relaxation of Highly Vibrationally Excited Pyrazine by CO_2. *J. Chem. Phys.* **1995**, *102*, 6032−6045.
(3) Weston, R. E., Jr.; Flynn, G. W. Relaxation of Molecules with Chemically Significant Amounts of Vibrational Energy: The Dawn of the Quantum State Resolved Era. *Annu. Rev. Phys. Chem.* **1992**, *43*, 559.
(4) Hippler, H.; Lindemann, L.; Troe, J. Collisional Energy Transfer of Vibrationally Highly Excited Molecules. V. UV Absorption Study of Azulene. *J. Chem. Phys.* **1985**, *83*, 3906−3912.
(5) Oref, I.; Tardy, D. C. Energy Transfer in Highly Excited Polyatomic Molecules. *Chem. Rev.* **1990**, *90*, 1407−1445.
(6) Flynn, G. W.; Parmenter, C. S.; Wodtke, A. M. Vibrational Energy Transfer. *J. Phys. Chem.* **1996**, *100*, 12817−12838.
(7) Mullin, A. S., Schatz, G. C., Eds. *Highly Excited Molecules: Relaxation, Reaction and Structure*; ACS Symposium Series 678; American Chemical Society: Washington, DC, 1996.
(8) Hold, U.; Lenzer, T.; Luther, K.; Reihs, K.; Symonds, A. C. Collisional Energy Transfer Probabilities of Highly Excited Molecules from Kinetically Controlled Selective Ionization (KCSI). I. The KCSI Technique: Experimental Approach for the Determination of P(E′,E) in the Quasicontinous Energy Range. *J. Chem. Phys.* **2000**, *112*, 4076−4089.
(9) Grigoleit, U.; Lenzer, T.; Luther, K.; Mützel, M.; Takahara, A. Collisional Energy Transfer of Highly Vibrationally Excited Toluene and Pyrazine: Transition Probabilities and Relaxation Pathways from KCSI Experiments and Trajectory Calculations. *Phys. Chem. Chem. Phys.* **2001**, *3*, 2191−2202.
(10) Hold, U.; Lenzer, T.; Luther, K.; Symonds, A. C. Collisional Energy Transfer Probabilities of Highly Excited Molecules from KCSI. III. Azulene: P(E′,E) and Moments of Energy Transfer for Energies up to 40,000 cm^{-1} via Self-calibrating Experiments. *J. Chem. Phys.* **2003**, *119*, 11192−11211.
(11) Liu, C.-L.; Hsu, H. C.; Hsu, Y. C. Energy Transfer of Highly Vibrationally Excited Naphtalene. I. Translational Collision Energy Dependence. *J. Chem. Phys.* **2007**, *127*, 104311.
(12) Du, J.; Sassin, N. A.; Havey, D. K.; Hsu, K.; Mullin, A. S. Full State-Resolved Energy Gain Profiles of CO_2 from Collisions with Highly Vibrationally Excited Molecules. II. Energy-Dependent Pyrazine (E=32700 and 37900 cm^{-1}) Relaxation. *J. Phys. Chem. A* **2013**, *117*, 12104−12115.
(13) Hold, U.; Lenzer, T.; Luther, K.; Reihs, K.; Symonds, A. Collisional Energy Transfer Probabilities in the Deactivation of Highly Vibrationally Excited Aromatics. *Ber. Bunsen-Ges. Phys. Chem.* **1997**, *101*, 552−565.
(14) Wall, M. C.; Mullin, A. S. Supercollision" Energy Dependence: State-resolved Energy Transfer in Collisions Between Highly Vibrationally Excited Pyrazine (E_{vib} = 37,900 cm^{-1} and 40,900 cm^{-1}) and CO_2. *J. Chem. Phys.* **1998**, *108*, 9658−9667.
(15) Wall, M. C.; Lemoff, A. S.; Mullin, A. S. Independent Determination of Supercollision Energy Loss Magnitudes and Rates in Highly Vibrationally Excited Pyrazine with E_{vib} = 36,000−41,000 cm^{-1}. *J. Phys. Chem. A* **1998**, *102*, 9101−9105.
(16) Pashutzki, A.; Oref, I. Collision-induced Dissociation of Cyclohexadiene by a Vibrationally Hot Collider. *J. Phys. Chem.* **1988**, *92*, 178−182.
(17) Liu, C.-L.; Hsu, H. C.; Lyu, J.-J.; Ni, C.-K. Supercollisions and Energy Transfer of Highly Vibrationally Excited Molecules. *J. Chem. Phys.* **2005**, *123*, 131102.
(18) Li, Z.; Sansom, R.; Bonella, S.; Coker, D. F.; Mullin, A. S. Trajectory Study of Supercollision Relaxation in Highly Vibrationally Excited Pyrazine and CO_2. *J. Phys. Chem. A* **2005**, *109*, 7657−7666.
(19) Clary, D. C.; Gilbert, R. G.; Bernshtein, V.; Oref, I. Mechanisms for Supercollisions. *Faraday Discuss.* **1995**, *102*, 423−433.
(20) Bernshtein, V.; Oref, I. Effect of Supercollisions on Chemical Reactions in the Gas Phase. *J. Phys. Chem.* **1993**, *97*, 12811−12818.
(21) Miller, L. A.; Barker, J. R. Collisional Deactivation of Highly Vibrationally Excited Pyrazine. *J. Chem. Phys.* **1996**, *105*, 1383−1391.
(22) Lendvay, G.; Schatz, G. C. Energy Dependence of Energy Transfer in the Collisional Relaxation of Vibrationally Highly Excited CS_2. *J. Phys. Chem.* **1991**, *95*, 8748−8753.
(23) Zalesskaya, G. A.; Yakovlev, D. L.; Sambor, E. G.; Prikhodchenko, D. V. Influence of Short- and Long-range Interaction Forces on the Efficiency of Collisional Vibrational Energy Transfer in the Vibrational Quasi-continuum. *Opt. Spectrosc.* **2001**, *90*, 596−603.
(24) Lim, K. F. Quasiclassical Trajectory Study of Collisional Energy Transfer in Toluene Systems. I. Argon Bath Gas: Energy Dependence and Isotope Effects. *J. Chem. Phys.* **1994**, *100*, 7385−7399.
(25) Lim, K. F. Quasiclassical Trajectory Study of Collisional Energy Transfer in Toluene Systems. II. Helium Bath Gas: Energy and Temperature Dependences, and Angular Momentum Transfer. *J. Chem. Phys.* **1994**, *101*, 8756−8767.
(26) Pan, B.; Bowman, J. M. Quantum Scattering Calculations of Energy Transfer and Dissociation of HCO in Collisions with Ar. *J. Chem. Phys.* **1995**, *103*, 9661−9668.
(27) Qi, J.; Bowman, J. M. Quantum Calculations of Inelastic and Dissociative Scattering of HCO by Ar. *J. Chem. Phys.* **1998**, *109*, 1734−1742.
(28) Dagdigian, P. J.; Alexander, M. H. Exact Quantum Scattering Calculations of Transport Properties: CH_2-He. *J. Chem. Phys.* **2013**, *138*, 164305.
(29) Jasper, A. W.; Miller, J. A. Collisional Energy Transfer in Unimolecular Reactions: Direct Classical Trajectories for $CH_4 \rightleftarrows CH_3$ + H in Helium. *J. Phys. Chem. A* **2009**, *113*, 5612−5619.
(30) Jasper, A. W.; Miller, J. A. Theoretical Unimolecular Kinetics for CH_4 + M $\rightleftarrows$ CH_3 + H + M in Eight Baths, M = He, Ne, Ar, Kr, H_2, N_2, CO, CH_4. *J. Phys. Chem. A* **2011**, *115*, 6438−6455.
(31) Jasper, A. W.; Miller, J. A.; Klippenstein, S. J. The Collision Efficiency of Water in the Unimolecular Reaction CH_4 (+H_2O) → CH_3 + H (+H_2O): One-Dimensional and Two-Dimensional Solutions of the Low-Pressure-Limit Master Equation. *J. Phys. Chem. A* **2013**, *117*, 12243−12255.
(32) Bruehl, M.; Schatz, G. C. Theoretical Studies of Collisional Energy Transfer in Highly Excited Molecules: Temperature and Potential Surface Dependence of Relaxation in He, Ne, Ar + CS_2. *J. Phys. Chem.* **1988**, *92*, 7223−7229.
(33) Martínez-Núñez, E.; Vázquez, S. A.; Marques, J. M. C. Quasiclassical Trajectory Study of the Collision-Induced Dissociation of CH_3SH^+ + Ar. *J. Chem. Phys.* **2004**, *121*, 2571−2577.
(34) Martínez-Núñez, E.; Fernández-Ramos, A.; Vázquez, S. A.; Marques, J. M. C.; Xue, M.; Hase, W. L. Quasiclassical Dinamycs Simulation of the Collision-Induced Dissociation of $Cr(CO)_6^+$ with Xe. *J. Chem. Phys.* **2005**, *123*, 154311.
(35) Duchovic, R. J.; Hase, W. L. A Dynamical Study of the H + CH_3 → CH_4 Recombination Reaction. *J. Chem. Phys.* **1985**, *82*, 3599−3606.
(36) Bernshtein, V.; Lim, K. F.; Oref, I. Temporal Dependence of Collisional Energy Transfer by Quasiclassical Trajectory Calculations of the Toluene-Argon System. *J. Phys. Chem.* **1995**, *99*, 4531−4535.
(37) Martínez-Núñez, E.; Vázquez, S. A. Classical Dynamics Study of the Unimolecular Decomposition of CH_3SH^+. *J. Phys. Chem. A* **1999**, *103*, 9783−9793.
(38) Grigoleit, U.; Lenzer, T.; Luther, K.; Mützel, M.; Takahara, A. Collisional Energy Transfer of Highly Vibrationally Excited Toluene and Pyrazine: Transition Probabilities and Relaxation Pathways from KCSI Experiments and Trajectory Calculations. *Phys. Chem. Chem. Phys.* **2001**, *3*, 2191−2202.
(39) Meroueh, O.; Hase, W. L. Collisional Activation of Small Peptides. *J. Phys. Chem. A* **1999**, *103*, 3981−3990.
(40) Brunsvold, A. L.; Garton, D. J.; Minton, T. K.; Troya, D.; Schatz, G. C. Crossed Beams and Theoretical Studies of the Dynamics of Hyperthermal Collisions Between Ar and Ethane. *J. Chem. Phys.* **2004**, *121*, 11702−11714.
(41) Lenzer, T.; Luther, K.; Troe, J.; Gilbert, R. G.; Lim, K. F. Trajectory Simulations of Collisional Energy Transfer in Highly Excited Benzene and Hexafluorobenzene. *J. Chem. Phys.* **1995**, *103*, 626−641.

(42) Lenzer, T.; Luther, K. Intermolecular Potential Effects in Trajectory Calculations of Collisions Between Large Highly Excited Molecules and Noble Gases. *J. Chem. Phys.* **1996**, *105*, 10944−10953.
(43) Charlo, D.; Clary, D. C. Quantum-mechanical Calculations on Termolecular Association Reactions (XY+Z+M) → (XYZ+M): Application to Ozone Formation. *J. Chem. Phys.* **2002**, *117*, 1660−1672.
(44) Xie, T.; Bowman, J. M. Quantum Inelastic Scattering Study of Isotope Effects in Ozone Stabilization Dynamics. *Chem. Phys. Lett.* **2005**, *412*, 131−134.
(45) Ivanov, M. V.; Babikov, D. Collisional Stabilization of van der Waals States of Ozone. *J. Chem. Phys.* **2011**, *134*, 174308.
(46) Ivanov, M. V.; Babikov, D. On Molecular Origin of Mass-independent Fractionation of Oxygen Isotopes in the Ozone Forming Recombination Reaction. *Proc. Natl. Acad. Sci.* **2013**, *110* (44), 17708−17713.
(47) Chen, C.; Braams, B.; Lee, D. Y.; Bowman, J. M.; Houston, P. L.; Stranges, D. Evidence for Vinylidene Production in the Photodissociation of the Allyl Radical. *J. Phys. Chem. Lett.* **2010**, *1*, 1875−1880.
(48) Huang, X.; Braams, B. J.; Bowman, J. M. ab initio Potential Energy and Dipole Moment Surfaces for $H_5O_2^+$. *J. Chem. Phys.* **2005**, *122*, 044308.
(49) Xie, Z.; Braams, B. J.; Bowman, J. M. Ab Initio Global Potential Energy Surface for $H_5^+ \rightarrow (H_3^+ H_2)$. *J. Chem. Phys.* **2005**, *122*, 224307.
(50) Chen, C.; Braams, B.; Lee, D. Y.; Bowman, J. M.; Houston, P. L.; Stranges, D. The Dynamics of Allyl Radical Dissociation. *J. Phys. Chem. A* **2011**, *115*, 6797−6804.
(51) Stranges, D.; Stemmler, M.; Yang, X.; Chesko, J. D.; Suits, A. G.; Lee, Y. T. UV Photodissociation Dynamics of Allyl Radical by Photofragment Translational Spectroscopy. *J. Chem. Phys.* **1998**, *109*, 5372−5382.
(52) Stranges, D.; O'Keeffe, P.; Scotti, G.; Di Santo, R.; Houston, P. L. Competing Sigmatropic Shift Rearrangements in Excited Allyl Radicals. *J. Chem. Phys.* **2008**, *128*, 151101.
(53) Lendvay, G.; Schatz, G. C. Observation of Highly Energetic Collisions in Classical Trajectory Studies of Collisional Energy Transfer. *J. Phys. Chem.* **1990**, *94*, 8864−8866.
(54) Han, Y.-C.; Sharma, A. R.; Bowman, J. M. Quasiclassical Trajectory Study of Fast H-atom Collisions with Acetylene. *J. Chem. Phys.* **2012**, *136*, 214313.
(55) Gilbert, R. G. Theory of Collisional Energy Transfer of Highly Excited Molecules. *Int. Rev. Phys. Chem* **1991**, *10*, 319−347.
(56) Boys, S. F.; Bernardi, F. The calculation of small molecular interactions by the differences of separate total energies. Some procedures with reduced errors. *Mol. Phys.* **1970**, *19*, 553−566.
(57) Varandas, A. J. C.; Rodrigues, S. P. J. Double Many-Body Expansion Potential Energy Surface for Ground-State HCN Based on Realistic Long Range Forces and Accurate ab initio Calculations. *J. Chem. Phys.* **1997**, *106*, 9647−9658.
(58) Rodrigues, S. P. J.; Varandas, A. J. C. Dynamics Study of the Reaction (Ar + HCN) → (Ar + H + CN). *J. Phys. Chem. A* **1998**, *103*, 6266−6273.
(59) *Mathematica*, Version 8.0; Wolfram Research, Inc.: Champaign, IL, 2010.
(60) Pirani, F.; Alberti, M.; Castro, A.; Moix Teixidor, M.; Cappelletti, D. Atom-bond pairwise additive Representation for Intermolecular Potential Energy Surfaces. *Chem. Phys. Lett.* **2004**, *394*, 37−44.
(61) Maitland, C. G.; Smith, E. B. A Simplified Representation of Intermolecular Potential Energy. *Chem. Phys. Lett.* **1973**, *22*, 443−446.
(62) Lendvay, G.; Schatz, G. C. Choice of Gas Kinetic Rate Coefficients in the Vibrational Relaxation of Highly Excited Polyatomic Molecules. *J. Phys. Chem.* **1992**, *96*, 3752−3756.
(63) Lendvay, G.; Schatz, G. C. Comparison of Master Equation and Trajectory Simulation of the Relaxation of an Ensemble of Highly Vibrationally Excited Molecules. *J. Phys. Chem.* **1994**, *98*, 6530−6536.
(64) Troe, J. Theory of thermal unimolecular reactions at low pressures. III. Superposition of weak and strong collisions. *J. Chem. Phys.* **1992**, *97*, 288−292.
(65) Porter, R. N.; Raff, L. M. In *Dynamics of Molecular Collisions*; Miller, W. H., Ed.; Plenum: New York, 1976; Vol. *B*.